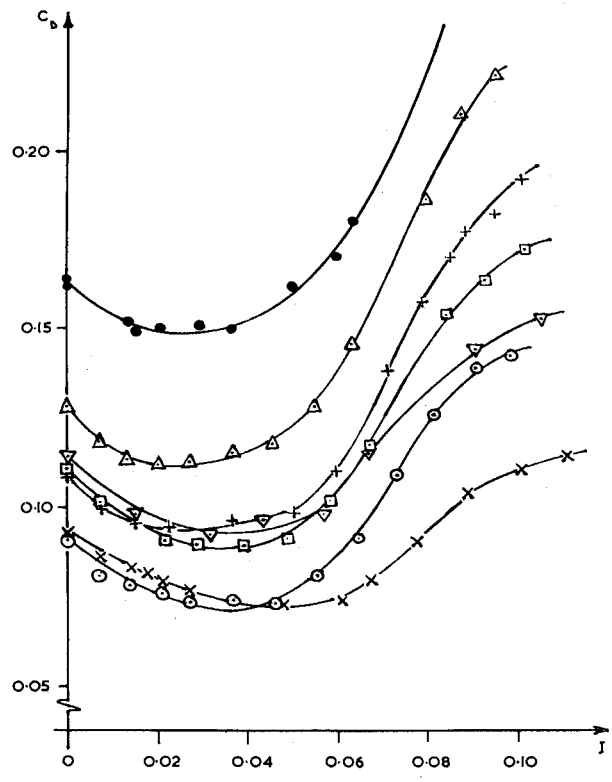

Fig. 5 Afterbody drag coefficient with jet flow, $M = 0.95$.

the nozzle exit) and the variation of C_D with M_∞ is shown in Fig. 3. At the largest values of β the boat-tail drag, which is mainly generated by supersonic expansion around the first shoulder, outweighs the benefit of the increase in recovered base pressure and the afterbody drag is generally higher than that acting on the 6° boat-tail of the same length. A cross-plot of C_D against β for the various Mach numbers showed that the optimum β for minimum afterbody drag through the transonic speed range and with no jet flow is $\beta \simeq 7°$ for $l = 0.5$ and 1.0. This is in agreement with the results of other workers at transonic speeds[3] and at $M_\infty = 2.0$[4].

Pressure distributions over eight afterbodies were measured at $M_\infty = 0.95$ with flow through the nozzle at mass flow rates (relative to stream conditions and centerbody section area) up to $I = 0.11$. The change in base pressure $\Delta C_{pb} = C_{pb}(I = 0) - C_{pb}(I)$ with flow rate I for the various afterbodies is shown in Fig. 4. Initially the base pressures increased with flow rate, but at higher flow rates the base pressure decreased rapidly, as has been indicated previously for cylindrical afterbodies.[2] At low flow rates ($I < 0.03$) Sykes[5] was unable to determine any significant difference in the variation of ΔC_{pb} with I due to differences in afterbody geometry, but the present data indicate that such differences do exist, particularly at the higher flow rates of these tests. It appears from Fig. 4 that, for engineering purposes, the base pressure change on the flare, cylindrical and 3° boat-tail models was almost the same; for $\beta = 6°$ and $\beta = 9°$ the base pressure changes each followed a similar but separate curve with increase of β and l resulting in higher pressure being recovered at slightly higher flow rates in the low flow rate region whilst at the higher flow rates the pressure defects were decreased.

The pressures on the afterbodies near the first shoulder where the flow was locally supersonic were not influenced by nozzle flow rate, but some influence was detected near the base where the flow was locally subsonic. The resulting variation of C_D with I was fairly small, the change being typically about 0.005, and these data were combined with the area-weighted base pressure coefficients (again assumed constant over the nozzle exit) to give afterbody drag coefficients C_D; the variation of C_D with I is shown in Fig. 5. It is immediately apparent from this figure that the adverse effect of higher nozzle flow rate on base pressure is greatly alleviated by boat-tailing, due to the combined beneficial effects of a reduced pressure change from a small pressure defect at zero flow acting on a reduced base area. It is also apparent that whilst at low flow rates the optimum boat-tail angle is about 7°, at higher flow rates the optimum angle is larger.

For cylindrical afterbodies, the variation of C_{pb} with the ratio of jet total pressure to freestream static pressure P_{0j}/P_∞ at $M_\infty = 0.95$ and 1.20 from the present tests has been compared with data of Kurn[2] at $M_\infty = 0.955$ and 1.17 with sonic nozzles having exit to base area ratio $Aj/A = 0.20$ and 0.30. The effect of increasing Aj/A is to increase the base pressure defect at the higher pressure ratios but to reduce the base pressure defect at the lower pressure ratios associated with base bleed conditions.

References

[1] Cubbage, J. M., "Jet Effects on Base and Afterbody Pressures of a Cylindrical Afterbody at Transonic Speeds," RM L56 C21, 1956, NACA.

[2] Kurn, A. G., "A Base Pressure Investigation at Transonic Speeds on an Afterbody containing Four Sonic Nozzles and a Cylindrical Afterbody containing a Central Sonic Nozzle," TN Aero. 2869, 1963, Royal Aircraft Establishment, Farnborough, England.

[3] Silhan, F. V. and Cubbage, J. M., "Drag of Conical and Circular Arc Boat-Tail Afterbodies at Mach Numbers from 0.6 to 1.3," RM L56 K22, 1957, NACA.

[4] Bowman, J. E. and Clayden, W. A., "Boat-tailed Afterbodies at $M = 2$ with Gas Ejection," *AIAA Journal*, Vol. 6, No. 10, Oct. 1968, pp. 2029–2030.

[5] Sykes, D. M., "Cylindrical and Boat-tailed Afterbodies in Transonic Flow with Gas Ejection," *AIAA Journal*, Vol. 8, No. 3, March 1970, pp. 588–590.

Effect of Yaw of Repose on Ballistic Match of Similar Projectiles

H. R. Vaughn* and G. G. Wilson†
Sandia Laboratories, Albuquerque, N. Mex.

Analysis

Yaw of repose results when a gyroscopically stable body is subjected to aerodynamic moments generated by flight path curvature. In a normal shell trajectory, the yaw of repose angle causes the nose of the shell to precess to the right and up from the trajectory for positive spin rates,[1–3] when viewing the shell from the rear (Fig. 1). This causes the shell to drift to the right and above the zero lift trajectory, al-

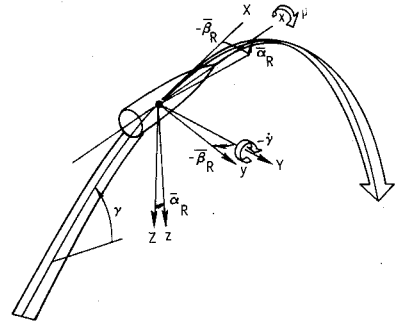

Fig. 1 Yaw of repose.

Received July 9, 1970; revision received February 19, 1971. This work was supported by the U.S. Atomic Energy Commission.

* Supervisor, Aeroballistics Division, Aerothermodynamics Projects Department. Associate Fellow AIAA.

† Member of the Technical Staff, Aeroballistics Division. Member AIAA.

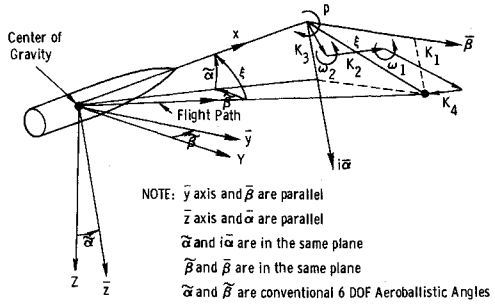

Fig. 2 Aeroballistic axis system.

though the drift due to $\bar{\beta}_R$ is usually much larger than the lofting due to $\bar{\alpha}_R$. This effect is of overriding importance in the ballistic matching of shells.

The aeroballistic axis system (Fig. 2) is used in this analysis, and only the yaw of repose part of the motion, K_4, is considered here, since the other parts of the motion have been more fully developed.[4–6] Consideration of the rigid-body moment equations of motion give a linear second-order nonhomogeneous differential equation of the form

$$\ddot{\xi} + N_1\dot{\xi} + N_2\xi = N_3e^{ipt} + N_4 \tag{1}$$

where N_1, N_2, N_3 and N_4 are all constants. The solution to this equation consists of

$$\xi = K_1e^{(\lambda_1+i\omega_1)t} + K_2e^{(\lambda_2+i\omega_2)t} + K_3e^{ipt} + K_4 \tag{2}$$

where

$$\lambda_{1,2} = [(M_q + M_{\dot{\alpha}})/(2I)]\{1 \pm (pI_x/2I)/[(pI_x/2I)^2 - (M_\alpha/I)]^{1/2}\} \pm \{(pI_x/2I)(M_{p\beta}/I_x)/[(pI_x/2I)^2 - (M_\alpha I)]^{1/2}\} \tag{3}$$

$$\omega_{1,2} = (pI_x/2I) \pm [(pI_x/2I)^2 - (M_\alpha/I)]^{1/2} \tag{4}$$

(In many instances it is desirable to include the effects of lift and drag on the damping factors and frequencies.)

The first three terms of Eq. (2) have been considered previously[3–5] and will not be further developed. The nutation, K_1, and precession, K_2, arms result from initial conditions and damp rapidly on a well-designed shell. The trim part of the motion, K_3, is usually not very important on a well-balanced shell, since the high roll rates generally reduce the nonrolling trim angle to a very small angle. This leaves the yaw of respose, K_4, as a very important parameter in ballistic matching, which is to be further developed. The yaw of repose is expressed by

$$K_4 = [-i\ddot{\gamma} - (p\dot{\gamma}I_x/I)]/[(\lambda_1 + i\omega_1)(\lambda_2 + i\omega_2)] \tag{5}$$

where

$$K_4 = \xi_R = i\bar{\alpha}_R + \bar{\beta}_R \tag{6}$$

It should be noted that $\dot{\gamma}$ is left arbitrary in Eq. (5), and consequently differs from forms available in literature.[1,4,5]

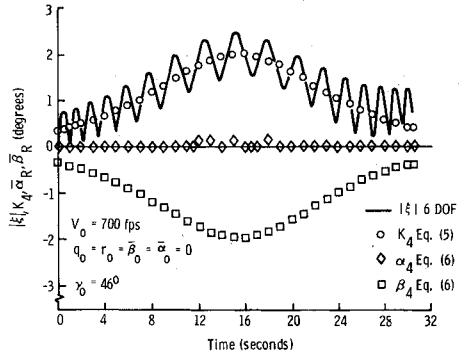

Fig. 3 Variation of yaw of repose components with trajectory time.

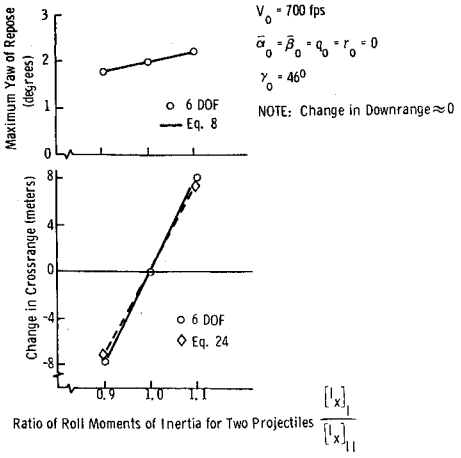

Fig. 4 Variation of yaw of repose components with trajectory time.

Peripheral computations of the four components of the angular motion were made during six-degree-of-freedom (6-dof) simulations of projectile trajectories. Comparisons between the equations for K_4, $\bar{\alpha}_R$, $\bar{\beta}_R$ and 6-dof calculations, which include the effects of gravity, lift, and drag on $\dot{\gamma}$, are shown for two trajectories in Figs. 3 and 4. The agreement is excellent.

Fortunately, it is possible to drastically simplify these expressions for most shell problems, because $\lambda_{1,2}$ are usually much smaller than $\omega_{1,2}$. Typically, $\lambda_{1,2} \sim (\frac{1}{2}\dot{0})\omega_2$, $\lambda_{1,2} \sim (\frac{1}{2}\dot{0}\dot{0})\omega_1, \omega_2 \sim (\frac{1}{1}\dot{0})\omega_1$. Consequently, useful approximate, but reasonably accurate, expressions for $\bar{\alpha}_R$ and $\bar{\beta}_R$ can be obtained by assuming $\lambda_1\lambda_2 \ll \omega_1\omega_2$ and $\lambda_1\omega_2 \ll \lambda_2\omega_1 \ll \omega_1\omega_2$. Also, $\ddot{\gamma}$ is usually very small compared with $p(I_x/I)\dot{\gamma}$ in any normal trajectory. Therefore,

$$\bar{\alpha}_R \cong (pI_x\dot{\gamma}\lambda_2/I)/(\omega_1\omega_2^2) \tag{7}$$

and

$$\bar{\beta}_R \cong (pI_x\dot{\gamma}/I)/(\omega_1\omega_2) \tag{8}$$

and since λ_2 may be typically $(\frac{1}{2}\dot{0})\omega_2$, $\bar{\alpha}_R \cong (\frac{1}{2}\dot{0})\bar{\beta}_R$. Consequently, the effect of $\bar{\alpha}_R$ on ballistic matching is usually much less important than $\bar{\beta}_R$. A further simplification can be made in the expression for $\bar{\beta}_R$ by substituting Eq. (4) into Eq. (8),

$$\bar{\beta}_R = (pI_x\dot{\gamma}/M_\alpha) = (pI_x\dot{\gamma})/[C_{N\alpha}q'S(X_{cg} - X_{cp})] \tag{9}$$

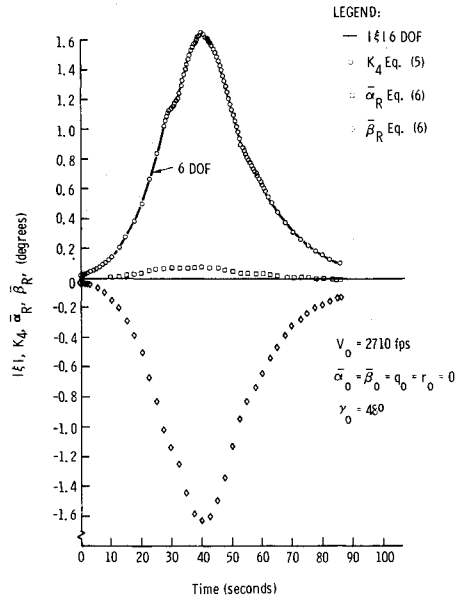

Fig. 5 Comparison of 6-dof claculation and theory.

Now, if one is attempting to ballistically match two shells (I and II) to be fired from the same gun,

$$\{I_x/[C_{N\alpha}(X_{cg} - X_{cp})]\}_I = \{I_x/[C_{N\alpha}(X_{cp} - X_{cg})]\}_{II} \quad (10)$$

is required if they are to traverse the same trajectory. If the two shells have essentially the same external shape,

$$[I_x/(X_{cg} - X_{cp})]_I = [I_x/(X_{cg} - X_{cp})]_{II} \quad (11)$$

for identical trajectories. The reader is reminded that while Eq. (10) or (11) is an overriding factor in ballistic matching, neither I_x nor X_{cg} can be changed unless the following conditions remain satisfied:

$$s = [(pI_x/2I)^2/(M_\alpha/I)] > 1, \quad \lambda_{1,2} < 0,$$
$$\text{and} \quad (C_D S/W)_I = (C_D S/W)_{II} \quad (12)$$

It is also desirable that $\lambda_{1,2}$ and $\omega_{1,2}$ be roughly matched so that the transient dynamic performance is not changed excessively. The fact that the drag-to-weight ratios must be matched [Eq. (12)] is assumed to be obvious.

Cross Range Drift

It is possible to integrate Eq. (9) when $\bar{\beta}_R$ is constant and obtain an expression for the cross range drift,

$$\mathfrak{D} \cong \iint - (gN_\alpha \bar{\beta}_R/W)dtdt = -(gN_\alpha \bar{\beta}_R/W)(t^2/2) \quad (13)$$

where $N_\alpha = (C_{N\alpha} q' S)$.

It can be shown that for a vacuum trajectory,

$$\dot{\gamma} \cong -g \cos\gamma_0/V_0 \quad (14)$$

$$t = 2V_0 \sin\gamma_0/g \quad (15)$$

and

$$V_0 = [gR/(2 \sin\gamma_0 \cos\gamma_0)]^{1/2} \quad (16)$$

Substitution of Eqs. (14–16) into Eq. (13) yields

$$\mathfrak{D} = pI_x(\sin\gamma_0)^{3/2}(2gR)^{1/2}(\cos\gamma_0)^{1/2}/[W(X_{cg} - X_{cp})] \quad (17)$$

where average values for p and $(X_{cg} - X_{cp})$ should be used. Although it is possible to estimate cross range drift of a shell from this equation, it is more useful in predicting the change in drift resulting from perturbations of the shell characteristics. For instance, if it is desired to examine the sensitivity of $\mathfrak{D}$ to changes in I_x, Eq. (17) becomes

$$\mathfrak{D} = CI_x \quad (18)$$

where C is evaluated by calculating a single nominal trajectory. This approach is shown in Fig. 5 compared with 6-dof simulation, and the agreement is excellent. The same approach can be taken with the other shell parameters.

Conclusions

The yaw of repose theory shows that the ratio of roll moment of inertia to the static margin predominates in controlling the yaw of repose angle magnitude in the usual projectile problem. Aside from the drag-to-weight ratio, which dominates any projectile ballistic match problem, the yaw of repose is the single most important projectile parameter.

References

[1] McShane, E. J., Kelley, J. L., and Reno, F. V., "Exterior Ballistics," University of Denver Press, 1953, pp. 625–631.

[2] Vaughn, H. R. and Wilson, G. G., "Yaw of Repose on Spinning Shells," SC-RR-70-155, Jan. 1970, Sandia Labs., Albuquerque, N. Mex.

[3] Nayfeh, A. H., unpublished work on the Dispersion of Reentry Vehicles Caused by Overspin, Aerotherm Corp., Mountain View, Calif., work done under contract to Sandia Corp., PR 48-7754.

[4] Nicolaides, J. D., "Free Flight Dynamics," Rept. 1966, Aero-Space Dept., Univ. of Notre Dame, Notre Dame, Ind.

[5] Murphy, C. H., "Free Flight Motion of Symmetric Missiles," Rept. 1216, July 1963, Ballistic Research Labs., Aberdeen Proving Ground, Md.

[6] Vaughn, H. R., "A Detailed Development of the Tricyclic Theory," SC-M-67-2933, Feb. 1968, Sandia Labs., Albuquerque, N. Mex.

Mass Transfer Effectiveness at Three-Dimensional Stagnation Points

A. WORTMAN*
Northrop Corporation, Hawthorne, Calif.
AND
A. F. MILLS†
University of California, Los Angeles, Calif.

Nomenclature

C = $(\rho\mu)/(\rho\mu)_e$
f_i = stream function such that $\partial f/\partial\eta = u_i/u_{i_e}$, $i = 1,2$
g = enthalpy ratio $H/H_e = h/h_e$
K = transverse to principal inviscid velocity ratio = α_2/α_1
M = molecular weight
Nu = Nusselt number, $q_s Pr_s x_1/(H_e - h_s)\mu_s$
q = surface conductive heat flux
u_i = velocity component
u = airspeed
x_i = coordinate; $i = 1,2$ along surface, $i = 3$ normal to surface
α_i = inviscid velocity gradient such that $u_{i_e} = \alpha_i x_i$, $i = 1,2$
λ = heat-transfer parameter, $C_s g_s'/(1 - g_s)Pr_s$
λ^* = heat-transfer parameter for zero mass transfer
Λ = normalized heat-transfer parameter, λ/λ^*
η = transformed coordinate, $(\rho_e\alpha_1/\mu_e)^{1/2}\int_0^{x_s}(\rho/\rho_e)d\tilde{x}_3$
ϕ = injection parameter, $-f_s/\lambda^*$
ω = exponent in viscosity-enthalpy relation

Subscripts

e = edge of boundary layer
i = injected species; coordinate direction
s = surface condition

PRESENTED in this Note are the results of a parametric study of the effectiveness of mass transfer in reducing heat transfer to regular three dimensional stagnation points. The shapes considered here possess two planes of symmetry and range from spheres, through cylinders, to saddle points with equal magnitudes of adverse and favorable pressure gradients. Calculations were performed for model gases ($\rho\alpha h^{-1}$, $\mu\alpha h^\omega$, Pr = const) for wall to total enthalpy ratios ranging up to 0.9, and using real air properties for enthalpy ratios of engineering interest. Our primary objective is to present a simple correlation function appropriate for engineering estimates of mass transfer effects over a wide range of shapes, enthalpy ratios, gas properties, and injection rates. By considering realistic model gases and real air properties in a systematic parametric study, the present contribution stresses heat transfer, in contrast to the study of Libby[1] which employed the simplifying assumption of $\rho\mu$ = const, and focused on enthalpy ratios of 0.0 and 1.0.

The present work follows on that presented in Ref. 2, where heat-transfer correlations were developed for the zero mass transfer situation. The governing equations for three dimensional stagnation point flows are taken directly from

Received November 9, 1970; revision received December 21, 1970.

* Engineering Specialist, Aerodynamics Research Branch. Member AIAA.

† Assistant Professor, School of Engineering and Applied Science. Member AIAA.